

Controlling Polymer Morphologies by Intramolecular and Intermolecular Dynamic Covalent Iron(III)/Catechol Complexation—From Polypeptide Single Chain Nanoparticles to Hydrogels

Marco Hebel, Jasmina Gačanin, Thorsten Lückerrath, David Y. W. Ng,* and Tanja Weil*

Responsive biomaterials, tunable from the molecular to the macroscopic scale, are attractive for various applications in nanotechnology. Herein, a long polypeptide chain derived from the abundant serum protein human serum albumin is cross-linked by dynamic-coordinative iron(III)/catechol bonds. By tuning the binding stoichiometry and the pH, reversible intramolecular folding into polypeptide nanoparticles with controllable sizes is achieved. Moreover, upon varying the stoichiometry, intermolecular cross-links become predominant yielding smart and tunable macroscopic protein hydrogels. By adjusting the intra- and intermolecular interactions, biocompatible and biodegradable materials are formed with varying morphologies and dimensions covering several lengths scales featuring rapid gelation without toxic reagents, fast and autonomous self-healing, tunable mechanical properties, and high adaptability to local environmental conditions. Such material characteristics can be particularly attractive for tissue engineering approaches to recreate soft tissues matrices with highly customizable features in a fast and simple fashion.

on concentration gradients or environmental stimuli. In various aspects, polymer chemists have taken a great deal of inspiration from nature, i.e., in creating supramolecular nanostructures of distinct shapes by single chain folding, which mimics folding processes of proteins or their assembly into larger superstructures.^[1–3] There is still great interest to expand the available chemical tools to control folding of a single polymer chain into nano-objects of distinct shapes and to lock these shapes by covalent cross-linking via condensation reactions, cycloaddition reactions (click chemistries), or dynamic covalent bonds such as hydrazones.^[1,4,5] In fact, dynamic covalent (DC) bonds play a crucial role in cellular life as they provide many attractive features such as controlled structure formation across hierarchies, stability in aqueous media and reversibility in response to external stimuli such as pH or redox environments.^[6] For instance,

disulfides stabilize proteins in their bioactive three dimensional shapes and reversible unfolding, i.e., denaturation facilitates digestion and cellular recycling.^[7] Apart from stabilization of the folded polypeptide chain at specific positions in the proteins structure, proteins could also be cross-linked by disulfides into the macroscopic fibrillar structures such as in keratin, which provides mechanic stability.^[8–10] Dynamic exchange of disulfide bonds proceeds either through enzymes like the protein disulfide isomerases and thioredoxins or in redox environments, allowing Nature to manipulate bio-architectures on demand. The ingenuity of controlling such a large repertoire of protein structures and assemblies by a single type of DC bond formation indicates that there is still great potential to apply such methods also for structure formation of polymeric materials in the synthetic world.^[11,12]


In this respect, DC reactions based on metal coordination chemistry offer many exciting features such as stable complex formation in physiological aqueous media, reversibility as well as the opportunity to record changes in the coordination sphere by optical readout. Due to the presence of a large coordination sphere and the variable oxidation states, metals such as iron(II)/iron(III) can often offer a higher level of design complexity. Catechols, for example, bind to iron(III) in a bidentate

1. Introduction

Nature's control of supramolecular systems across structural hierarchies from the molecular to the macroscopic range ubiquitously drives cellular processes and structure formation. Controlled supramolecular interactions form the basis for biorecognition as they allow dynamic binding and dissociation based

M. Hebel, J. Gačanin, T. Lückerrath, T. Weil
 Institute of Inorganic Chemistry I
 Ulm University
 Albert-Einstein-Allee 11, Ulm 89081, Germany
 E-mail: weil@mpip-mainz.mpg.de

J. Gačanin, T. Lückerrath, D. Y. W. Ng, T. Weil
 Max Planck Institute for Polymer Research
 Ackermannweg 10, Mainz 55128, Germany
 E-mail: david.ng@mpip-mainz.mpg.de

 The ORCID identification number(s) for the author(s) of this article can be found under <https://doi.org/10.1002/marc.202100413>

© 2021 The Authors. Macromolecular Rapid Communications published by Wiley-VCH GmbH. This is an open access article under the terms of the Creative Commons Attribution License, which permits use, distribution and reproduction in any medium, provided the original work is properly cited.

DOI: 10.1002/marc.202100413

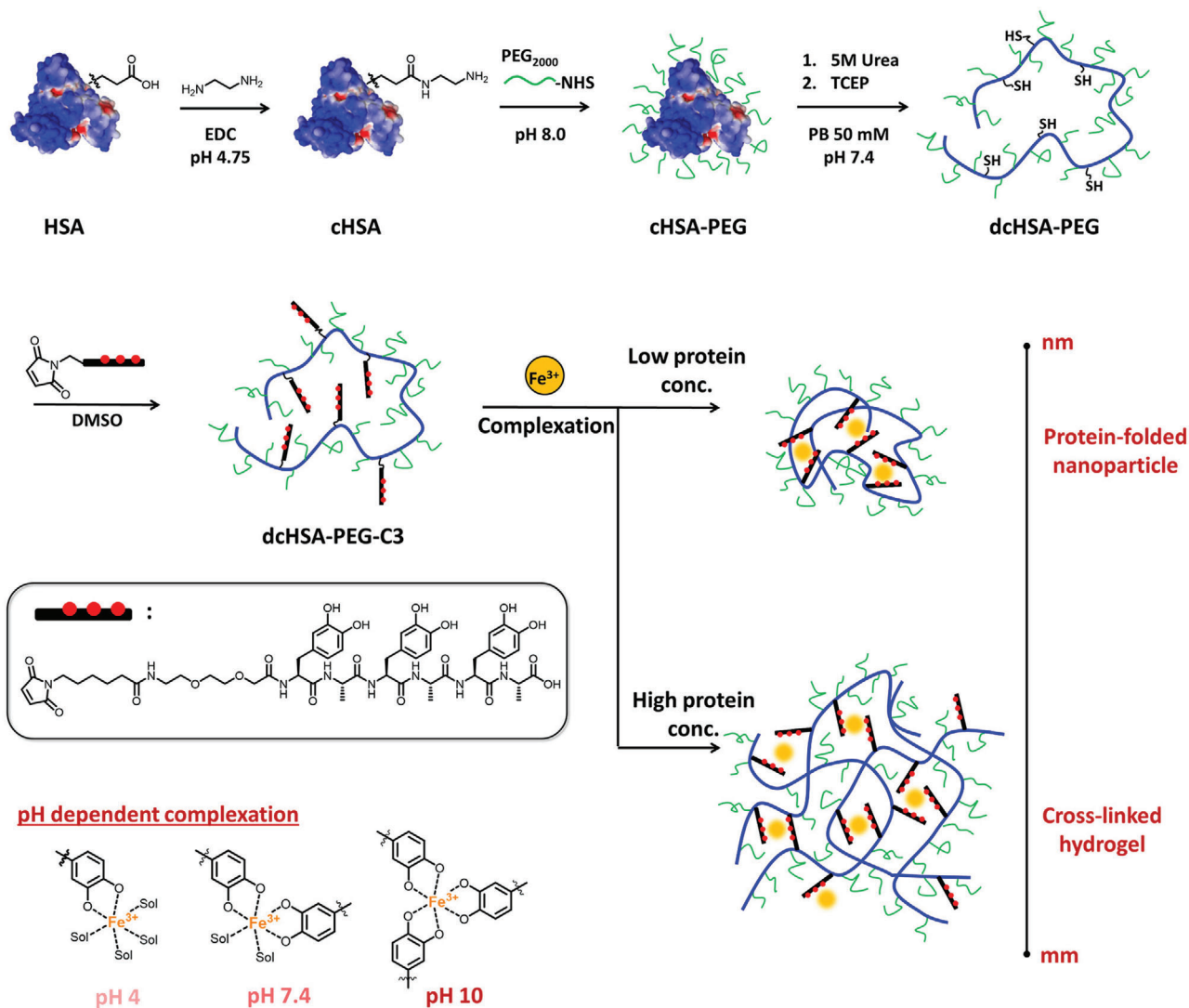


Figure 1. Synthesis route to the biopolymer dcHSA-PEG-C3 and the resulting formation of protein-folded nanoparticles or cross-linked protein hydrogels, pH dependent coordination of iron(III) to the catechol groups in aqueous solution.

format in an octahedral geometry where mono-, bis- and tris-catechol coordination is determined simply by pH. Compared to many other reversible motifs such as synthetic hydrogen bonding units, e.g. boronic acid/diol complexation, the association constants of iron(III)/catechol complexes in buffer are several orders of magnitude higher in the range of $\log K_a \approx 50$.^[13–16] As such, the iron(III)/catechol interaction offers distinct advantages for the formation of traceable and reversible DC complexes that remain stable even under physiological conditions.

Inspired by the versatility of DC bonds in Nature, we report the formation of polypeptide nanoparticles that are converted into hydrogels through dynamic covalent complex formation. The polypeptide sequence of the abundant blood plasma protein human serum albumin (HSA) was modified by introducing catechol groups as new dynamic interaction points so that the polypeptide backbone folds intramolecularly into polypeptide nanoparticles (Figure 1). By varying the iron(III)/catechol stoichiometry and/or pH, or concentration, a hydrogel was formed.

In this way, we show that the integration of coordination chemistry into macromolecular architectures provides a versatile toolbox that allows facile access to tuneable biomaterials or nanostructures, even under physiological conditions. These biocompatible and biodegradable materials could be of interest for various applications in biological systems due to their rapid gelation without toxic reagents, fast and autonomous self-healing, tunable mechanical properties and high adaptability to local environmental conditions. Such characteristics could be particularly attractive for tissue engineering approaches to recreate different soft matrices in a fast and simple fashion without the necessity to modify the system.

2. Results and Discussion

The HSA protein provides a long polypeptide sequence with high numbers of reactive lysine, aspartic and glutamic acid groups as well as 35 cysteines that could be easily modified.

Moreover, globular HSA could be denatured easily in the presence of chaotropic agents and under reductive conditions.^[17,18] HSA was first cationized with ethylenediamine and PEGylated with PEG₂₀₀₀-NHS ester ($\approx 2000 \text{ g mol}^{-1}$) in order to stabilize the protein backbone and to prevent aggregate formation and precipitation during disulfide reduction as reported previously.^[17,18] Characterized by MALDI-TOF MS, an average of 22 PEG₂₀₀₀-NHS ester were attached to HSA (Supporting Information).

Denaturation of the protein backbone by 5 M urea and tris(2-carboxy-ethyl)phosphine (TCEP)^[18] exposes the reduced sulfhydryl groups of the cysteine residues for subsequent thiol-Michael addition with C3, a maleimide-terminated oligopeptide with three catechol repeats that serves as anchor groups for the formation of DC metal complexes. The new catechol units are well-positioned at the locations of the 35 cysteine groups due to the chemoselectivity of the maleimide-thiol reaction in polar organic solvents.^[19,20] After purification by size exclusion chromatography, **dcHSA-PEG-C3** was isolated and functionalization was quantified by applying the fluorescence chemosensor, 2-anthraceneboronic acid, whose interaction with catechols results in quenching of its fluorescence, which was used to determine the number of C3 per **dcHSA-PEG** (Supporting Information). A maximum of 18 sulfhydryl groups were functionalized by applying C3 in excess, corresponding to approximately 54 catechol groups attached to the HSA amino acid sequence (Figure 2b).

Coordination of iron(III) to the catechol functionalized biopolymer **dcHSA-PEG-C3** was assessed by UV-vis absorption spectroscopy for varying complex stoichiometries and pH values (Figure 2d). Different amounts of iron(III) (conc. $\approx 3.1 \text{ mM}$) were titrated to **dcHSA-PEG-C3** at pH 4, 7.4, and 10 (Figures S1–S3, Supporting Information). At pH 10, a characteristic absorbance of the tris-catechol iron(III) complex $[\text{Fe}(\text{cat})_3]^{3-}$ was detected at $\approx 475 \text{ nm}$.^[21] At pH 7.4, the predominant catechol-iron(III) species $[\text{Fe}(\text{cat})_2]^-$ appeared with an absorption at 540 nm, along with a minor presence of $[\text{Fe}(\text{cat})_3]^{3-}$. The small shoulder at 710 nm indicated the presence of a monovalent complex $[\text{Fe}(\text{cat})]^+$.^[21,22] At pH 4, no prominent peaks were observed in the visible range. These observations are consistent with experiments on different catechol-iron species in the literature, whose proportions change dynamically with pH.^[21] In order to control complex formation both intra- and intermolecularly, the interaction and coordination extent between iron(III) and catechols on the protein was optimized by UV-vis spectroscopy. By varying the amount of iron(III) from 0 to 360 mol equiv., the highest absorbance at 540 nm was recorded at 180 equiv. indicating the majority of iron(III) existing as bis-catechol iron(III) complexes (Figure S3, Supporting Information). At 360 mol equiv. of iron(III), the equilibrium of the iron-catechol complexes shifts slightly towards the monovalent complex as excess iron(III) competes for coordination thereby reducing the absorbance of the bis-complex (Figure S3, Supporting Information).

Under very dilute conditions ($0.7 \times 10^{-9} \text{ M}$), we expect the system to favor intramolecular complexation to afford single chain nanoparticles (Figure 2). In order to reduce secondary interactions of the polypeptide backbone, complexation of iron(III) was accomplished in 8 M urea to minimize aggregative forces during chain folding. To investigate the folding process, different amounts of iron(III) were added into a solution of **dcHSA-PEG-**

C3 ($0.7 \times 10^{-9} \text{ M}$) at pH 4, 7.4 and 10. The formation of single chain polypeptide nanoparticles was monitored by dynamic light scattering (DLS) and size-exclusion chromatography (SEC) (Figure 3, Supporting Information). Under non-complexation conditions at pH 4, there was no change in the hydrodynamic diameter of $27 \pm 0.1 \text{ nm}$ regardless of the quantity of the iron(III) added. At pH 7.4, the hydrodynamic diameter of **dcHSA-PEG-C3** revealed a gradual reduction from $25 \pm 0.7 \text{ nm}$ (for iron(III) $> 7.5 \text{ mol equiv.}$) to $19 \pm 0.5 \text{ nm}$ (for 30 mol equiv., Figure 3; Figure S5, Supporting Information). This suggests that at least 7.5 mol equiv. of iron(III) were required to produce a detectable change in the hydrodynamic size of the polypeptide. At 30 mol equiv. of iron(III), full coordination to the catechol groups was achieved. In comparison to the experimental results, we estimated the expected size (R) of the single chain nano particles formed from dynamic covalent iron(III)/catechol interactions at pH 7.4. The calculation according to Pomposo et al.^[23] gives 24.5 nm and 23.6 nm for 10 equiv. or 30 equiv. of iron(III), respectively (Supporting Information). The smaller experimental values suggest that the trimeric arrangement of the catechols might have caused a stronger mechanical binding of the chains and hence greater compactness than predicted. Comparatively, at pH 10, the size distribution increased by $5 \pm 0.5 \text{ nm}$ with increasing amounts of iron(III), promoting inter-particle interactions due to the increase in coordination number.

Considering the dimensions of PEGylated proteins, our data suggests that single chain nanoparticles are formed and multi-chain aggregates are unlikely. The average hydrodynamic diameter of native HSA is approximately 7 nm, but it is known that the attachment of PEG chains of various sizes further increases the hydrodynamic radius of proteins significantly, which has been reported for other protein-PEG conjugates such as lysozyme, shown to drastically increase the hydrodynamic size to 45–50 nm.^[24,25] In contrast, multi-chain protein particles of HSA-PEG conjugates have demonstrated to reach diameters above 80 nm.^[26,27] From this perspective, the size of **dcHSA-PEG-C3** in the presence of iron(III) at pH 7.4 do not seem to indicate the aggregation of multiple protein chains in a single particle.

These size differences observed in DLS were subsequently verified independently using size-exclusion chromatography (Figure 3d,e). At pH 7.4, the retention time of **dcHSA-PEG-C3** was successively increased from 28 to 29 min upon the addition of 0 equiv. to 30 equiv. of iron(III). This correlation suggests that the addition of higher amounts of iron(III) reduces the hydrodynamic volume of the nanoparticles. At pH 10, the nanoparticles showed a larger size and hence a reduction in the retention time from 30 to 28.4 min with increasing amounts of iron(III), complementing the DLS measurements. However, at pH 4, the conjugate was retained on the column and could not be eluted most likely due to the interaction between the mono-catechol-iron(III) complexes and the dextran material of the column.

Taken together, the results of the DLS and SEC indicate that the observed reduction in the hydrodynamic volume of **dcHSA-PEG-C3** by iron(III)/catechol complexation originates from intramolecular cross-linking. In particular, higher ordered aggregates caused by inter-particle cross-linking were not detected by DLS and SEC at pH 7.4. Even at pH 10, given the capacity for further coordination and cross-link, the detected size increase was unexpectedly defined. In contrast, at pH 4, iron(III) and catechol

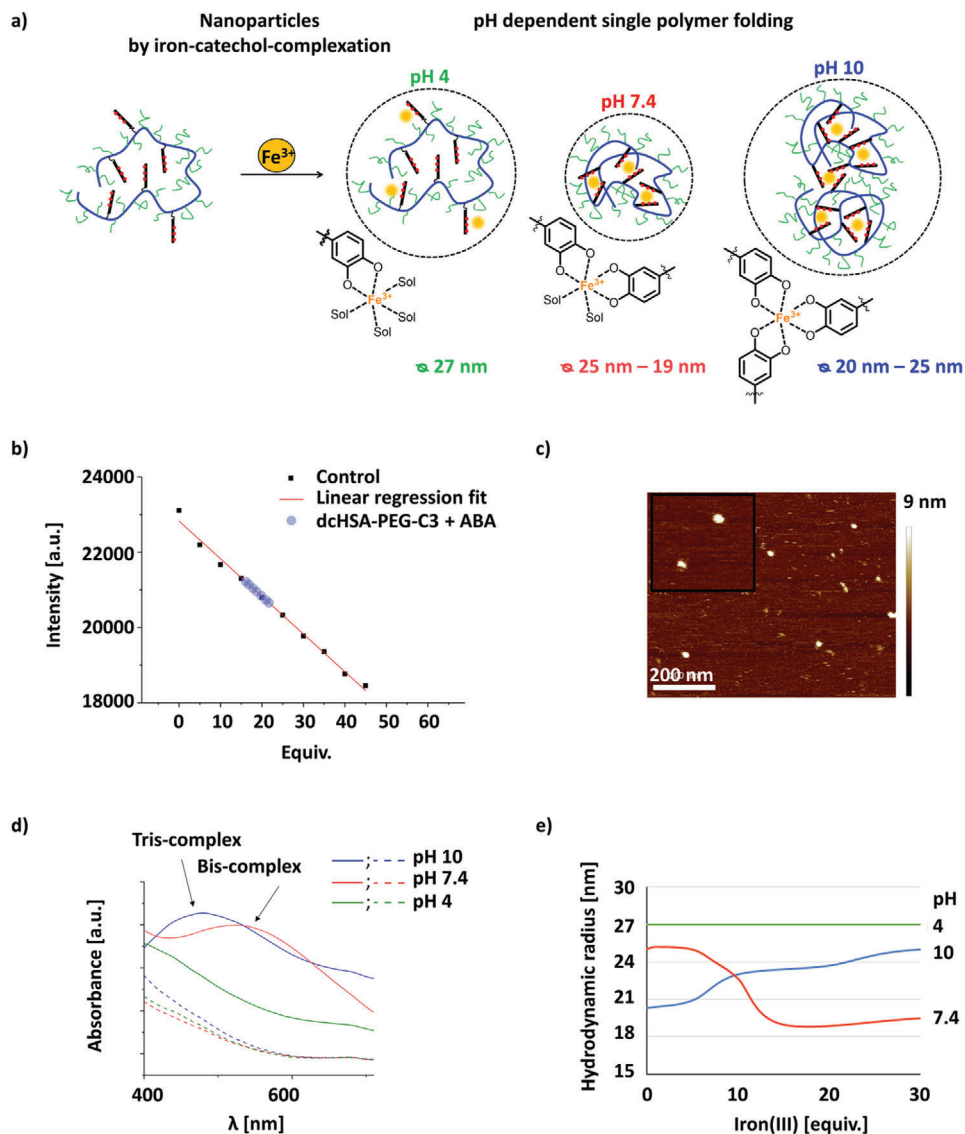


Figure 2. a) Visualization of **dcHSA-PEG-C3** of the single polymer folding process with pH dependent folding of nanoparticles by iron-catechol-complexation. Under non-complexation conditions at pH 4, no change in the hydrodynamic diameter occurs regardless of the quantity of the iron(III). However, at pH 7.4 the quantity of added iron(III) determines the nanoparticle size, whereas at pH 10 inter-particle interactions are promoted. b) Measurement of the amount of catechol functionalities on **dcHSA-PEG-C3** with an 2-anthracene boronic acid chemosensor assay. The x-axis shows the equivalents of the catechol groups per molecule **dcHSA-PEG-C3**. The experiment was repeated several times resulting in an average of 18 catechol peptide molecules (54 catechol groups) per molecule **dcHSA-PEG-C3**. c) AFM image of **dcHSA-PEG-C3** nanoparticles. d) UV-vis absorbance spectra of **dcHSA-PEG-C3** mixed with iron(III) at different pH values (blue: pH 10, red: pH 7.4, green: pH 4, solid lines: 0 equiv. iron(III), dashed lines: 30 equiv. iron(III)). e) Correlation of the hydrodynamic radius of **dcHSA-PEG-C3** with the amount of iron(III) at pH 4, 7.4 and 10, measured by DLS.

formed predominantly a 1:1 complex, which resulted in a linear chain without any cross-linking.

While the conversion of polypeptide architectures to form intramolecular interactions was adjusted by tuning the amount of iron(III) and pH (Figure 2), intermolecular cross-links become dominant by increasing the concentration of the components. The formation of the hydrogels was observed by mixing 4 and 8 wt% of **dcHSA-PEG-C3** with water at pH 4, 7.4, and 10 and by adding different amounts of iron(III)-solution. Twelve different protein hydrogels consisting of precisely adjusted amounts of iron(III) at different pH values and weight percentages were

synthesized and their rheological properties were characterized (Table 1, Figure 4).

The mechanical properties, the storage moduli (G') and loss moduli (G'') of different gels were investigated in time-sweep experiments (Figure 4b; Figures S7–S9, Supporting Information, Table 1) with fixed frequency and strain (1%, 1 Hz). No crossover point of G' and G'' was observed throughout the measurement, indicating instant gelation during sample preparation (≈ 30 s) and constant gel stability over time. With 4 wt% of **dcHSA-PEG-C3** and 45 equivalents of iron(III) at pH 7.4, the material began to show gel-like properties as the storage modulus (G') was higher

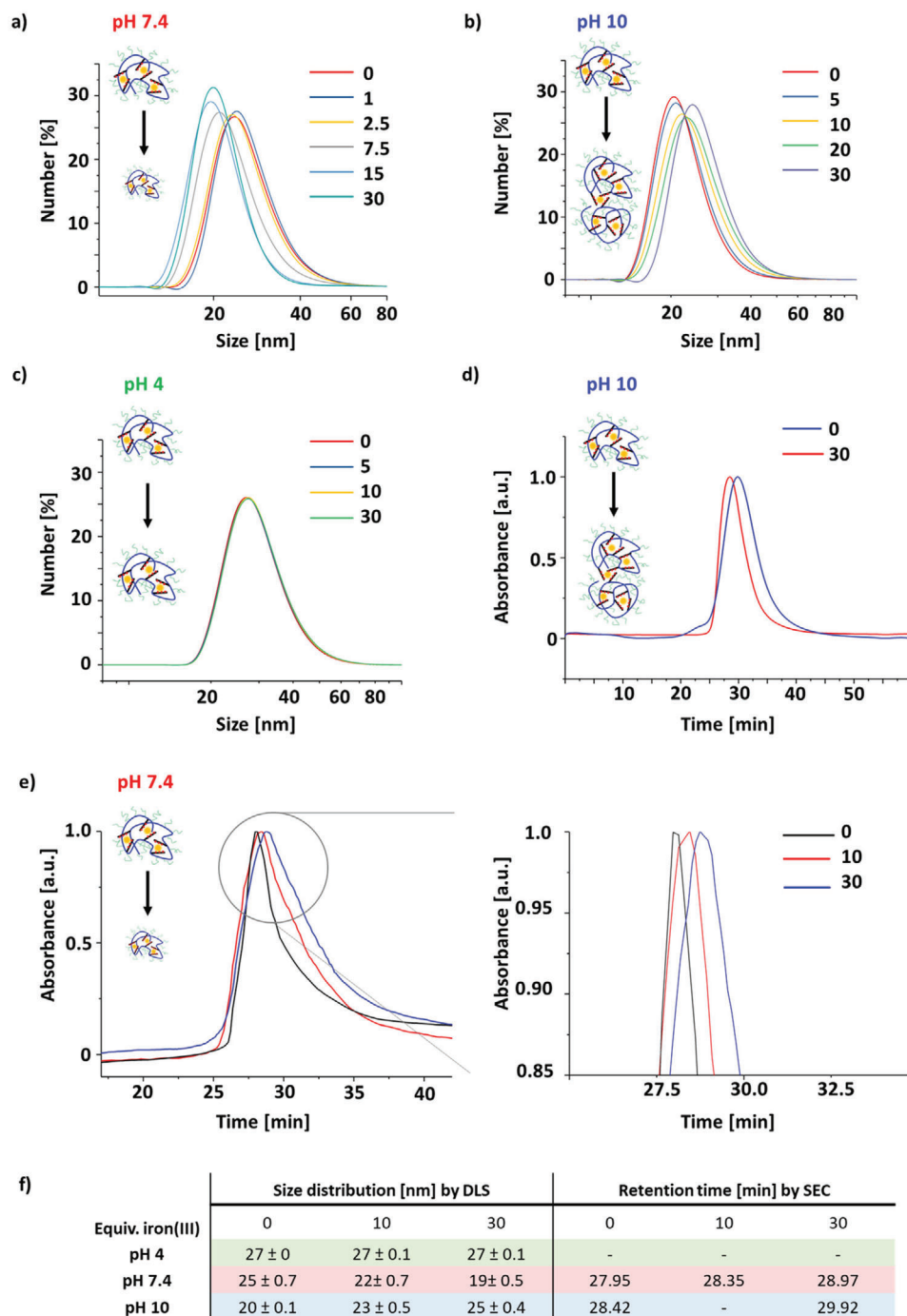


Figure 3. Hydrodynamic size distributions obtained by DLS for **dcHSA-PEG-C3** with different amounts of iron(III) (equiv.) at a) pH 7.4, b) pH 10, and c) pH 4. SEC chromatograms for **dcHSA-PEG-C3** with different amounts of iron(III) (equiv.) at d) pH 10 and e) pH 7.4, f) table of nanoparticle size distributions and retention times, measured by DLS and SEC.

than the loss modulus (G''). Further time-sweep experiments of the gels at pH 4, 7.4, and 10, independent of the amounts of polymeric material, showed that higher amounts of iron(III) resulted in higher G' , indicating a higher cross-link density. This observation is consistent with the results of the UV-vis experiments, which also demonstrated higher cross-linking of the bis- and tris-catecholato-iron(III) complexes. At pH 4, the

material demonstrated storage and loss moduli of very soft gels ($G' \approx 10$ Pa) with liquid like behaviour (H1) because of the missing coordinative cross-linking structures. At pH 10, the gels were more robust according to their mechanical strength ($G' \approx 120$ Pa; H11) as the coordination density increases to accommodate up to three catechols (Figure 4b). Although increasing the number of interactions naturally leads to more stable structures,

Table 1. List of produced hydrogels (H1–H12) with different amounts of iron(III), weight percentage (wt%) of dcHSA-PEG-C3, pH values, including the analyzed rheological parameters storage moduli G' and loss moduli G'' (strain 1%, frequency 1 Hz), the self-healing properties (quantified by combined measurements of an oscillatory strain sweep (0.01–1000%, frequency 1 Hz) with subsequent oscillatory time sweep measurement (strain 0.1%, frequency 1 Hz)), and gel-to-sol transition points (strain sweeps (0.01–1000%), frequency 1 Hz). (–) = n.d., not determined.

	H1	H2	H3	H4	H5	H6	H7	H8	H9	H10	H11	H12
Equiv. iron(III)	45	90	180	180	45	90	180	180	45	90	180	180
Vol. [iron(III) sol.] [μL]	0.5	1	2	4	0.5	1	2	4	0.5	1	2	4
wt%	4	4	4	8	4	4	4	8	4	4	4	8
G' [Pa]	liquid	9	9	139	7	189	562	4359	–	15	118	2194
G'' [Pa]	liquid	4	1	10	3	37	92	573	–	3	12	132
Self-healing [%]	–	–	–	94 ± 8	–	60 ± 0	62 ± 1	84 ± 14	–	–	81 ± 19	–
Gel-sol-point [strain %]	–	–	–	254 ± 1	–	31 ± 0	35 ± 0	58 ± 7	–	–	118 ± 22	101 ± 2
		pH 4				pH 7.4				pH 10		

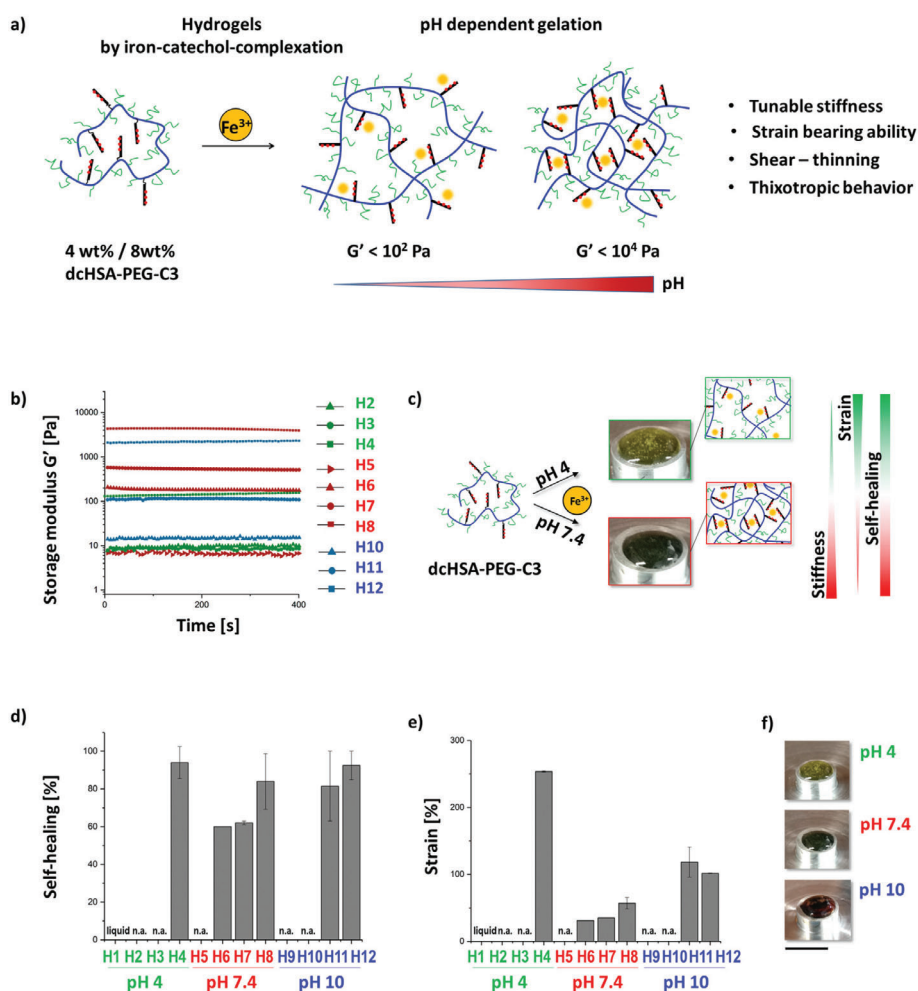


Figure 4. a) Schematic presentation of iron(III)-induced gelation of dcHSA-PEG-C3 and pH dependent cross-linking. b) Rheological measurements of produced hydrogels (H) with different amounts of iron(III), weight percentage of dcHSA-PEG-C3 and pH values. Comparison of different storage moduli G' with fixed strain (1%) and frequency (1 Hz), loss moduli are listed in Figures S7–S9 in the Supporting Information, c) Schematic illustration of pH dependent iron(III)-induced gelation and the resulting adjustability of hydrogel properties, showcasing hydrogels formed at pH 4 (e.g., H4) or pH 7.4 (e.g., H8) differing in their mechanical properties. d) Quantification of the self-healing properties of H1–H12 (combined measurements of an oscillatory strain sweep (0.01–1000%, frequency 1 Hz) with subsequent low strain oscillatory time sweep measurement (strain 0.1%, frequency 1 Hz)). e) Gel-to-sol transition points of H1–H12, measured by strain sweeps (0.01–1000%) at fixed frequency of 1 Hz. f) Photographs of iron(III)-induced hydrogels at different pH. Scale bar is 8 mm.

it is interesting to note that bis-complexes have been reported to exhibit higher mechanical strength than the tris-complexes.^[28,29] Indeed, according to the results of the storage and loss moduli, a higher mechanical strength of the bis-complexes dominated at pH 7.4 compared to the tris-complexes at pH 10. A higher amount of polymeric material also had a strong strengthening effect, as G' and G'' of the gels with 8 wt% material were 6 to 10 times higher than the gels with 4 wt%. The gels with the highest storage moduli reached G' of around 4300 Pa, which is comparable to the stiffness of liver tissue.^[30] The cross-linked gel was further characterized by frequency sweeps, but no frequency dependence for both G' and G'' between to 0.05–10 Hz and only a small continuous increase without intersection at higher frequencies was observed (Figure S11, Supporting Information).

Subsequently, the self-healing properties of the hydrogels were evaluated by consecutive measurements of strain sweeps up to strains of 1000% with the gels showing shear-thinning behavior and reaching a liquid-like state ($G' < G''$). This was followed by subsequent time sweeps with low fixed strain (0.1%) which allowed the monitoring of thixotropic behavior and recovery of the gel state ($G' > G''$), both at a fixed frequency of 1 Hz. The hydrogel self-healing is quantified (expressed as %) by the storage modulus G' of the respective gels using two sequential plateaus that flank a strain cycle. Very fast recovery rates of 60% to 100% of the gel's storage moduli were observed after removal of high shear force, even though no resting period was given after each step-strain experiment (Figure 4d, Table 1, Supporting Information), indicating the possibility of minimally-invasive administration of the gels via injection. Moreover, thixotropic behavior with excellent self-healing is highly beneficial for tissue engineering approaches where hydrogels need to enable, adapt, and recover from body movement or forces exerted on the material by cells or tissue. The gels at pH 4 (H1-H4) with a larger proportion of flexible and more dynamic cross-linking bonds, e.g., weak electrostatic forces between catechol and iron(III), showed higher recovery rates which is comparable to known literature.^[31] It has been shown before that dynamically cross-linked polyesters showed characteristic vitrification properties and usually demonstrated quantitative self-healing features.^[32] At higher pH values (pH 7.4 and pH 10) more coordinative cross-linking occurs and high recovery rates were observed, indicating a high reversibility of the stable bis- and tris-catecholato-iron(III) complexes.

The hydrogel mechanical properties showed a dependency on the applied strain during strain sweeps up to strains of 1000% where the gels showed a shear-thinning behavior (Supporting Information). Here, the strain values of the hydrogels (Figure 4e, Table 1), varying from 30% to 250%, mark the gel-to-sol transition, from which the system begins to act like a liquid. The differences can be attributed to the extent of coordination of catechols towards iron(III): at pH 4, mono-complexation dominates, whereas at pH 7.4 and 10, higher ordered complexes favors the establishment of strong interchain coordinative bonds. In comparison to other similar catechol-iron-based hydrogel systems, the gels described herein demonstrated high self-healing values without given healing time^[21,33,34] as well as the ability to bear high strain values of more than 100% up to the gel-to-sol transition (Figure 4, Table 1), which is significantly larger than iron(III)/catechol induced^[21] or telechelic bifunctional polymer-induced^[35] hydrogels from biopolymers.

3. Conclusion

We have demonstrated folding of a long polypeptide chain of HSA into nanoparticles or hydrogels based on intra- or intermolecular dynamic covalent bond formation and pH responsive iron(III)/catechol interactions. By dynamic covalent intermolecular cross-linking at low concentrations within the subnanomolar regime, single chain polypeptide nanoparticles with tunable sizes between pH 7.4 and 10 were achieved, based on the coordination level of iron(III). At high concentrations (> 4 wt% dHSA-PEG-C3), where interchain coordinative cross-linking was favored, macroscopic hydrogel matrixes with varying mechanical strength from $G', G'' = 0$ Pa to $G' = 4.4$ kPa, $G'' = 0.6$ kPa were obtained by simply adjusting the pH and the amount of iron(III) featuring rapid gelation without toxic reagents, fast and autonomous self-healing, tunable mechanical properties and high adaptability to local environmental conditions.

Given the ease of adjustability of mechanical properties, these hydrogels could be particularly useful for biomedical approaches, where stiffness, gel-to-sol transitions, and self-healing are major key parameters for successful integration of artificial cell matrices, drug delivery platforms, and their respective application routes, such as spray, injection, or implantation, e.g., via endoscopic routes. As such, systems like H4 that are able to gelate in an acidic environment without toxic catalysts, could be attractive for the promotion of gastrointestinal mucosal healing, which could be of interest for the prevention of ulcer-related complications.^[36] Hydrogels like H8 on the other side are highly attractive as artificial cell matrices with a broad relevance in various tissue engineering approaches.

Supporting Information

Supporting Information is available from the Wiley Online Library or from the author.

Acknowledgements

M.H. and J.G. contributed equally to this work. The authors acknowledge the financial support from the Deutsche Forschungsgemeinschaft (DFG, German Research Foundation) - project number 316249678 - SFB 1279 (C01), the Federal Ministry of Education and Research of Germany (BMBF) in the framework of ProMatLeben Polymere (InGel-NxG; Project number 13XP5086F), and the Max Planck–Bristol Centre for Minimal Biology.

Open access funding enabled and organized by Projekt DEAL.

Conflict of Interest

The authors declare no conflict of interest.

Data Availability Statement

The data that supports the findings of this study are available in the supplementary material of this article.

Keywords

albumin hydrogels, albumin nanoparticles, dynamic covalent materials, iron complexes, single chain folding, stimulus-responsiveness

Received: July 2, 2021
Revised: August 20, 2021
Published online: September 13, 2021

- [1] O. Altintas, C. Barner-Kowollik, *Macromol. Rapid Commun.* **2016**, *37*, 29.
- [2] O. Altintas, C. Barner-Kowollik, *Macromol. Rapid Commun.* **2012**, *33*, 958.
- [3] G. M. T Huurne, A. R. A. Palmans, E. W. Meijer, *CCS Chem.* **2019**, 64.
- [4] D. E. Whitaker, C. S. Mahon, D. A. Fulton, *Angew. Chem., Int. Ed.* **2013**, *52*, 956.
- [5] E. Verde-Sesto, A. Arbe, A. J. Moreno, D. Cangialosi, A. Alegría, J. Colmenero, J. A. Pomposo, *Mater. Horiz.* **2020**, *7*, 2292.
- [6] J. Li, P. Nowak, S. Otto, *J. Am. Chem. Soc.* **2013**, *135*, 9222.
- [7] M. Radzinski, T. Oppenheim, N. Metanis, D. Reichmann, *Biomolecules* **2021**, *11*, 469.
- [8] R. D. B. Fraser, T. P. Macrae, L. G. Sparrow, D. A. D. Parry, *Int. J. Biol. Macromol.* **1988**, *10*, 106.
- [9] G. Bulaj, *Biotechnol. Adv.* **2005**, *23*, 87.
- [10] I. Bosnjak, V. Bojovic, T. Segvic-Bubic, A. Bielen, *Protein Eng., Des. Sel.* **2014**, *27*, 65.
- [11] P. J. Hogg, *Trends Biochem. Sci.* **2003**, *28*, 210.
- [12] K. M. Cook, P. J. Hogg, *Antioxid. Redox Signal.* **2013**, *18*, 1987.
- [13] W. R. Harris, C. J. Carrano, K. N. Raymond, *J. Am. Chem. Soc.* **1979**, *101*, 2213.
- [14] M. Hebel, A. Riegger, M. M. Zegota, G. Kizilsavas, J. Gačanin, M. Pieszka, T. Lückerrath, J. A. S. Coelho, M. Wagner, P. M. P. Gois, D. Y. W. Ng, T. Weil, *J. Am. Chem. Soc.* **2019**, *141*, 14026.
- [15] A. W. Bosnian, L. Brunsveld, B. J. B. Folmer, R. P. Sijbesma, E. W. Meijer, *Macromol. Symp.* **2003**, *201*, 143.
- [16] G. Springsteen, B. Wang, *Tetrahedron* **2002**, *58*, 5291.
- [17] J. Gačanin, A. Kovtun, S. Fischer, V. Schwager, J. Quambusch, S. L. Kuan, W. Liu, F. Boldt, C. Li, Z. Yang, D. Liu, Y. Wu, T. Weil, H. Barth, A. Ignatius, *Adv. Healthcare Mater.* **2017**, *6*, 1700392.
- [18] J. Gačanin, J. Hedrich, S. Sieste, G. Glaßer, I. Lieberwirth, C. Schilling, S. Fischer, H. Barth, B. Knöll, C. V. Synatschke, T. Weil, *Adv. Mater.* **2019**, *31*, 1805044.
- [19] D. P. Nair, M. Podgórski, S. Chatani, T. Gong, W. Xi, C. R. Fenoli, C. N. Bowman, *Chem. Mater.* **2014**, *26*, 724.
- [20] A. B. Lowe, *Polym. Chem.* **2010**, *1*, 17.
- [21] J. Lee, K. Chang, S. Kim, V. Gite, H. Chung, D. Sohn, *Macromolecules* **2016**, *49*, 7450.
- [22] P. Sánchez, N. Gálvez, E. Colacio, E. Miñones, J. M. Domínguez-Vera, *Dalton Trans.* **2005**, *34*, 811.
- [23] J. A. Pomposo, J. Rubio-Cervilla, A. J. Moreno, F. Lo Verso, P. Bacova, A. Arbe, J. Colmenero, *Macromolecules* **2017**, *50*, 1732.
- [24] T. Zhao, Y. Yang, A. Z. Zong, H. N. Tan, X. L. Song, S. Meng, C. X. Song, G. L. Pang, F. S. Wang, *BioSci. Trends* **2012**, *6*, 81.
- [25] Y. R. Gokarn, M. Mclean, T. M. Laue, *Mol. Pharmaceutics* **2012**, *9*, 762.
- [26] J. G. Mehtala, C. Kulczar, M. Lavan, G. Knipp, A. Wei, *Bioconjugate Chem.* **2015**, *26*, 941.
- [27] Y. Wu, T. Wang, D. Y. W. Ng, T. Weil, *Macromol. Rapid Commun.* **2012**, *33*, 1474.
- [28] Y. Li, J. Wen, M. Qin, Yi Cao, H. Ma, W. Wang, *ACS Biomater. Sci. Eng.* **2017**, *3*, 979.
- [29] Z. Xu, *Sci. Rep.* **2013**, *3*, 2914.
- [30] M. A. Green, R. Sinkus, S. C. Gandevia, R. D. Herbert, L. E. Bilston, *NMR Biomed.* **2012**, *25*, 852.
- [31] P. S. Yavvari, A. Srivastava, *J. Mater. Chem. B* **2015**, *3*, 899.
- [32] W. Denissen, J. M. Winne, F. E. Du Prez, *Chem. Sci.* **2016**, *7*, 30.
- [33] P. S. Yavvari, S. Pal, S. Kumar, A. Kar, A. K. Awasthi, A. Naaz, A. Srivastava, A. Bajaj, *ACS Biomater. Sci. Eng.* **2017**, *3*, 3404.
- [34] C. Seidler, D. Y. W. Ng, T. Weil, *Tetrahedron* **2017**, *73*, 4979.
- [35] W. Xie, Q. Gao, Z. Guo, D. Wang, F. Gao, X. Wang, Y. Wei, L. Zhao, *ACS Appl. Mater. Interfaces* **2017**, *9*, 33660.
- [36] X. Xu, X. Xia, K. Zhang, A. Rai, Z. Li, P. Zhao, K. Wei, Li Zou, B. Yang, W.-K. Wong, P. W.-Y. Chiu, L. Bian, *Sci. Transl. Med.* **2020**, *12*, eaba8014.